Indian Journal of Pure & Applied Physics
Vol. 59, May 2021, pp. 404-411

Surface Evolution and Fractal Dimensions of $CH_3NH_3PbI_{3-X}Cl_X$ Thin Films and its Photovoltaic Performance

M S Patel[a], R P Yadav[b] & Lokendra Kumar[a*]

[a]Molecular Electronics Research Laboratory, Physics Department, University of Allahabad, Prayagraj-211 002, U P, India
[b]Department of Physics, Deen Dayal Upadhyay Govt. P.G. College,
Saidabad, Prayagraj- 221 508, India

Received 18 February 2021; accepted 6 April 2021

We fabricated the $CH_3NH_3PbI_{3-X}Cl_X$ perovskite crystalline films by solution processed method in air and nitrogen ambience to investigate the impact of the growth conditions on surface morphology and interface properties of the films. The surface morphology of $CH_3NH_3PbI_{3-X}Cl_X$ thin films are captured by scanning electron microscopy (SEM) and fractal analysis is performed on SEM micrographs. The value of fractal dimension/hurst exponent is found to be larger/smaller in N_2 environment as comparison to open air environment. The greater value of fractal dimension is corresponding to larger surface jaggedness which plays a crucial role for improving the interface between the perovskite and hole transportation layer. Furthermore, this analytical prediction is confirmed by photovoltaic devices fabricated on these films and observed a 60% enhancement in power conversion efficiency (PCE) of N_2 environment based thin films as compare to open air processed films. This may be due to the formation of compact and voids free perovskite self-affine fractal surfaces under nitrogen environment as compare to open air environment. Our findings represent a step forward to the realization of the peculiar morphological behaviour of the mixed halide perovskite fabricated in different environmental conditions.

Keywords: $CH_3NH_3PbI_{3-X}Cl_X$; environmental effect; fractal dimension; Hurts exponent; solar cell

1 Introduction

In past few years, hybrid of organic and inorganic halide perovskites has become very important for research in photovoltaic devices. These perovskite materials exhibit favourable optoelectronic properties such as high absorption coefficients, long electron-hole diffusion length, ambipolar charge transport and easy fabrication method. Testified power conversion efficiency (PCE) of perovskite solar cells (PSCs) were boosted from 3.8% to 25.2%[1-5]. However, some technical issues like toxicity and long term stability in ambient environment limit their commercialization. Perovskite film processing methods and environmental conditions play an important role to achieving high PCE[6-11]. The PCE of PSCs is very sensitive to humidity, oxygen, temperature and solvent vapours which prohibited their fabrication in ambient atmosphere [12-15]. In ambient condition, the interaction of humidity and oxygen with perovskite crystals minimizes the surface coverage of perovskite films and PCE. To avoid the adverse effects of moisture and oxygen, most of the highly efficient devices are being fabricated in glove box below the ppm level[16-17]. In glove box, the solvent evaporation achieves high super saturation which enhances the surface coverage and PCE of perovskite films. The effect of humidity on the nucleation of perovskite crystal is quite different at both spin coating stage as well as at the annealing stage. The quality of perovskite films can be controlled by changing the spin coating and annealing conditions[18-20]. Gao *et al.* reported that moisture reveals positive effect on crystal growth at annealing stage but adverse effect on the nucleation at the spin coating stage which causes poor film coverage[18]. Wang *et al.* reported enhanced PCE for vacuum annealed perovskite thin films devices[19]. According to Raga *et al.* the perovskite thin films fabricated in ambient conditions have better performance that of N_2 environment[20]. So, in order to fabricate highly efficient optoelectronic devices, it is essential to have deep understanding of surface morphology and control growth of perovskite films. The crystal growth of films on any substrate is random *i.e.* it varied from point to point which indicate the fractal nature of surface and can be theoretically calculated in terms of fractal dimension using scale invariant fractal analysis technique[21-25].

*Corresponding Author: lkumarau@gmail.com

For the theoretical investigations of surface morphology, several techniques like power spectral density (PSD), detrended fluctuation analysis (DFA) and Higuchi algorithm have been used[26-28]. Among them, the Higuchi algorithm gains much popularity in the various fields of science and technology. This algorithm has been used to investigate the Earth's geomagnetic motion, brain dynamics by using the electroencephalographic (ECG) signals, human emotions and the effect of the external periodic stressor on electrical oscillations in the brain[29-32]. In our previous report, we have applied this algorithm on AFM micrographs of different types of thin films for the determination of fractal dimension and Hurts exponent[23-24, 33]. Recently, this algorithm has been applied on the SEM micrographs of Cu doped $Sr(OH)_2$ thin films to calculate the fractal dimension and hurts exponent[34]. They developed a correlation between fractal dimension and specific capacity.

In the field of organic-inorganic hybrid perovskite materials some research group also investigated that the optoelectronic properties of perovskite films changes with fractal morphology. Huang *et al.* reported that fractal dimension and PCE of perovskite films increases with increasing the annealing time by using grazing-incidence small-angle scattering and wide-angle scattering (GISAXS/GIWAXS) techniques[21]. A similar study has been carried out by Liao *et al*. which indicate that a fractal pore network is developed inside the perovskite grains which provide a percolation path for the transportation of charge carriers[35]. Zhang *et al.* reported that the PSCs fabricated on a rough interface have better PCE in comparison to planar interface[36]. These investigations show that the morphology of perovskite films consists of fractal surface which significantly correlated with the performance of PSCs.

Here, we have investigated the effects of environmental conditions on the growth of perovskite crystal and their impact on the photovoltaic performance of PSCs in conventional device architecture with P3HT as HTL. The devices were fabricated by using $CH_3NH_3PbI_{3-X}Cl_X$ mixed halide perovskite material through one step spin coating methods in different environment. The structural, optical, electrical and morphological properties of perovskite thin films have been carried out. Moreover, Higuchi algorithm has been applied on SEM micrograph of both the films grown in open air environment and in N_2 environment to study the fractal morphology of $CH_3NH_3PbI_{3-X}Cl_X$ surface. The fractal dimension and hurts exponent has been calculated. For perovskite films, the correlations between fractal dimension, hurts exponent with their optical, electrical and morphological properties have been explored.

2 Materials and Methods

2.1 Materials and device fabrication

Synthesis of TiO_2 and MAI, pattering and cleaning of fluorine doped tin oxide (FTO) coated glass substrates were done according to previous reports[4]. Afterwards the pre cleaned and patterned substrates were placed in vacuum oven at 100°C for 20 min. Later TiO_2 layer was deposited by spin coating the TiO_2 precursor solution at 2000 rpm for 30 s followed by two step annealing process first heated at 120 °C for 10 min and then at 450 °C for 60 min to get compact TiO_2 (c-TiO_2) layer. Then, the some c-TiO_2 coated FTO substrates were transferred into N_2 filled glove box (O_2<0.5ppm and H_2O<0.5ppm) and some of them retained outside the glove box in relative humidity (RH) 45 (±2) % where perovskite layer was obtained by one step spin coating method. The two separate solution of $CH_3NH_3PbI_{3-X}$ Cl_X precursor was obtained by mixing 2.4 M of MAI and 0.8 M of $PbCl_2$ in anhydrous N, N-Di methyl formamide (DMF). One is stirred in open air environment of relative humidity (RH) 45 (±2) % and other is stirred in N_2 environment overnight at 70°C to obtained homogeneous precursor solution. The perovskite precursor solution was spin coated on the top of c-TiO_2 coated substrates at 4000 rpm for 30 s and annealed at 90 °C for 90 min. Thereafter, on top of $CH_3NH_3PbI_{3-X}Cl_X$ layer a hole transport layer of P3HT (16 mg/ml in chlorobenzene) was spin coated at 2000 rpm for 60 s (see Fig. 1a). Then on top of HTL layer Ag electrodes of thickness 100 nm were deposited at deposition rate 0.2–0.5 Å/sec and base pressure of 1×10^{-6} torr using shadow masks.

Figure 1(a) shows the schematic diagram for the fabrication of perovskite and P3HT films via spin coating technique. Firstly, perovskite precursor solution was spin coated on the pre-coated FTO/c-TiO_2 substrates and annealed at 90 °C for 90 min to get compact $CH_3NH_3PbI_{3-X}Cl_X$ perovskite films. Thereafter, P3HT was deposited on the top of perovskite films. Figure 1(b) shows the device architecture of perovskite solar cell FTO/c-TiO_2/$CH_3NH_3PbI_{3-X}Cl_X$/P3HT/Ag. The FTO coated

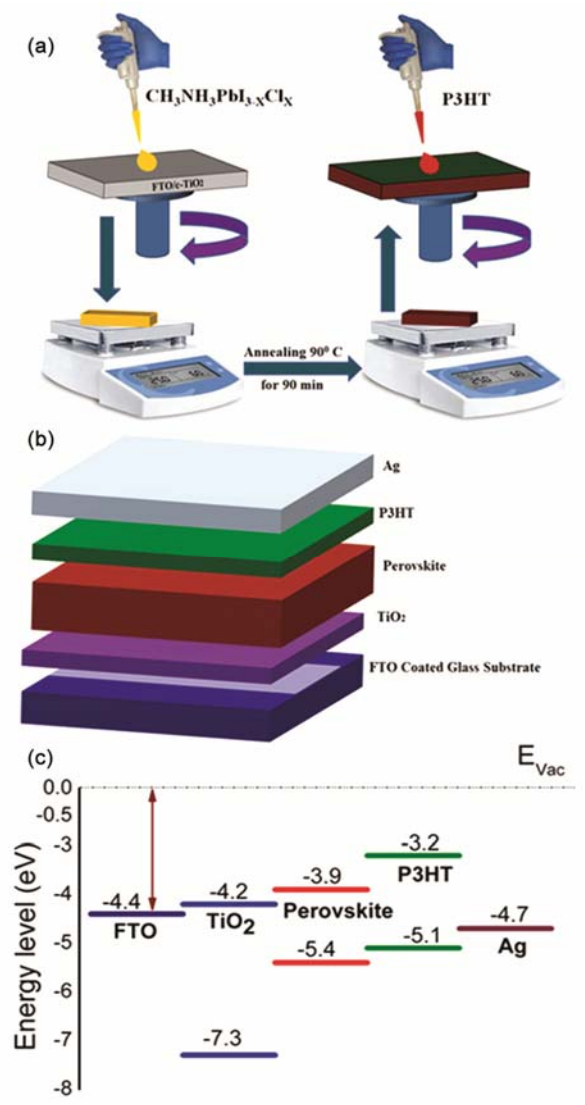

Fig. 1 — (a) Schematic diagram to grow perovskite and P3HT thin films (b) schematic diagram of complete perovskite solar cell and (c) energy level diagram of devices.

glass substrates work as transparent bottom electrode, c-TiO_2 works as an ETL, $CH_3NH_3PbI_{3-X}Cl_X$ works as photoactive layer, P3HT works as HTL and Ag works as top electrode. Figure 1(c) shows the energy level diagram of devices. The devices are illuminated from FTO side and light is absorbed by photoactive layer and electron-hole pairs are generated. These photo generated electron and hole pairs are collected by their respective electrodes *via* electron and hole transport layers.

2.2 Characterizations

The surface morphology of the perovskite films were investigated using Zeiss-Field Emission Scanning Electron Microscope (FE-SEM). *Image J* image processing software was used for the estimation of perovskite grain size from SEM micrographs. The structural characterization of the perovskite films were studied using Proto A-XRD Diffractometer equipped with CuK_α (λ= 1.54 Å) radiation. UV–Vis absorption (EA) spectra of the films were obtained using Unicam 5625 UV–Vis spectrometer. Photoluminescence (PL) spectra of the films were recorded in steady-state using Horiba Fluorolog equipped with a 450 W Xenon lamp excitation source. Current density–voltage (J–V) characteristic of the devices were performed under simulated AM 1.5 sunlight (100 mW/cm^2), from Photo Emission Technology, USA (PET-SS50AAA-EM), a class AAA solar simulator integrated with a Keithley 2400 source meter.

2.3 Fractal concept and Higuchi algorithm

The deposited thin films have irregular structures and surface height varies from point to point. These variations are responsible for surface roughness. Classically, the surface morphology of a thin film is measured in term of average roughness (R_a) and interface width (σ). Since both parameters are related to the roughness[24,34]. But these parameters provide only vertical properties such as top and valley variation of the surface; they do not give any information about the correlation and irregularity of the surface, which is an important characteristic of the surface[37]. Here, Higuchi algorithm is used as a direct method for calculating the fractal dimension of SEM micrographs. It is a very efficient method for directly estimating the fractal dimension. In this process the height of each pixel of a horizontal section of the surface is denoted by X(1), X(2).....X(N). The k subsequences have been constructed such as[33,34]

$$X_m^k = X(m), X(m+k), X(m+2k) \ldots\ldots\ldots\ldots X(m+pk) \quad \ldots (1)$$

where, m= 1, 2, 3,……., k and $p = int\left[\frac{N-m}{k}\right]$.

The length $L_m(k)$ of each segment Z_m^k is then given by

$$L_m(k) = \frac{\sum_{i=1}^{p}\left[|X(m+ik) - X\{m+(i-k)k\}|\frac{N-1}{p^k}\right]}{k} \quad \ldots (2)$$

where, $\frac{N-1}{p^k}$ is the normalization constant and N indicates the complete set of the sample points. The average value of length has been defined as:

$$L(k) = \frac{\sum_{m=1}^{k} L_m(k)}{k} \quad \ldots (3)$$

L(k) scales with k according to the power law as given below

$$L(k) \sim k^{-D_f} \quad \ldots (4)$$

Where, D_f is the fractal dimension. The estimation of the fractal dimension D_f has been obtained from the slope of log L(k) versus log k graph. The following relation has been used for obtaining the Hurst exponent, H, using the fractal dimension[23]

$$H = 2 - D_f \quad \ldots (5)$$

H is the measurement or complexity or irregularity of thin film surface at a certain scale.

3 Results and discussion

Figure 2 (a-b) shows the scanning electron microscope (SEM) micrographs of $CH_3NH_3PbI_{3-X}Cl_X$ mixed halide perovskite films fabricated in open air and N_2 environment respectively. The magnified view of same is shown in their respective insets. From SEM micrographs, it is clear that the compact, dense and voids free perovskite thin films are formed in N_2 environment with smaller grain size in comparison to open air environment. Due to high relative humidity in open air, new nucleation is rarely formed while in case of N_2 environment, the fast solvent evaporation creates new nucleation easily. This nucleation in perovskite crystal linked with neighbouring grains at spin coating stage, resulting in the formation of voids free high coverage perovskite surface. The grain size was calculated from the SEM Image with the help of Image J, image processing software and found to be in the range of 10-20 µm and 250- 900 nm for the perovskite films fabricated in open air and N_2 environment respectively. Although the grain size in open air environment is larger than N_2 environment but it consists of large voids of the order of 1-4 µm. These studies were depending on pictorial observation of SEM micrographs. For the deeper insight into the surface morphological investigations, we have used the Higuchi algorithm on SEM micrographs of perovskite films fabricated in different environment because the surface of SEM micrographs shows the self-affine fractal nature[38]. Higuchi algorithm is applied for fractal analysis of the SEM micrograph. Figure 3(a-b) shows the variation of log L(k) Vs. log k for $CH_3NH_3PbI_{3-X}Cl_X$ films grown in different environment. The slope of log L(k) Vs log k plot determines the fractal dimension of the surfaces. The average value of D_f was found to be 1.5561 ± 0.0549 and 1.8498 ± 0.0321 for $CH_3NH_3PbI_{3-X}Cl_X$ films grown in open air and N_2 environment respectively. The estimated value of D_f is larger for films grown in N_2 environment in comparison to open air condition which suggest that formation of rougher surfaces. These rougher surfaces of $CH_3NH_3PbI_{3-X}Cl_X$ films are very important factor that can improve the interfacing between $CH_3NH_3PbI_{3-X}Cl_X$ and P3HT layers[36]. The improvement in interfaces create a percolation path way for charge transportation which leads to the increment in current density from 20.40 to 22.5 mA/cm^2 along with fill factor from 0.476 to 0.547. The Figure 4(a-b) depicts the variation of D_f with the pixels for the $CH_3NH_3PbI_{3-X}Cl_X$ films fabricated in open air and N_2 environment respectively. From the variation it is clear that the $CH_3NH_3PbI_{3-X}Cl_X$ films grown in N_2 environment has maximum variations in

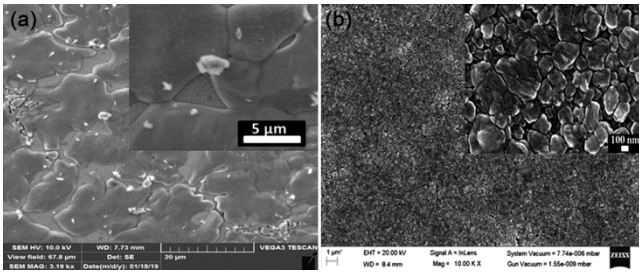

Fig. 2 — SEM images of the perovskite thin films fabricated on FTO substrate in (a) open air environment and (b) N_2 environment

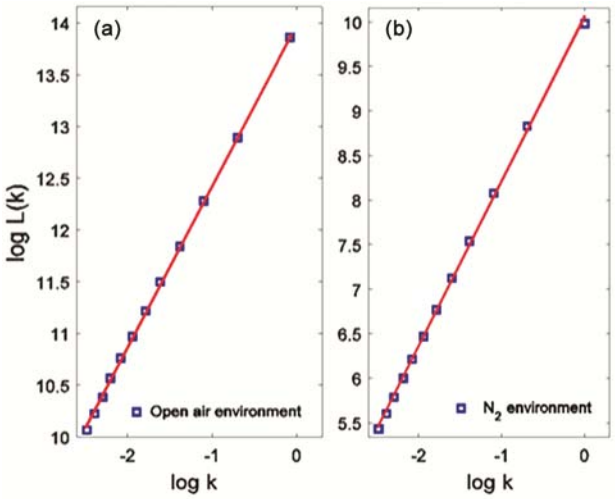

Fig. 3 — The variation of log L(k) as a function of log k for perovskite surface fabricated in (a) open air environment and (b) N_2 environment.

comparison to that of open air environment indicating that it has rougher surface. Figure 4(c-d) shows the variation of H with the row pixels for $CH_3NH_3PbI_{3-X}Cl_X$ thin films grown in open air and N_2 environment respectively. It was found that the $CH_3NH_3PbI_{3-X}Cl_X$ thin films grown in N_2 environment have smaller H value in comparison to that grown in open air environment. In both the cases, the H value was below 0.5 which indicates the anti-persistent behaviour[22,34]. The Hurst exponent (H) can be estimated by putting the value of D_f in Eq. 5 and found to be 0.4439 ± 0.0549 and 0.1502 ± 0.0321 for open air and N_2 environment respectively. H is the measurements of irregularity (complexity) of the thin film at a certain scale. Normally, H lies in the range $0 \leq H \leq 1$[22,34]. When the value of H, $0 \leq H \leq 0.5$ then the systems represent the anti-persistent behaviour and negatively correlated with surface heights at adjacent pixels while $0.5 \leq H \leq 1$ represents persistent behaviour and positively correlated with surface heights at adjacent pixels. Whereas, H =0.5 shows the height variations at any pixel are independent of height variations in adjacent pixels.

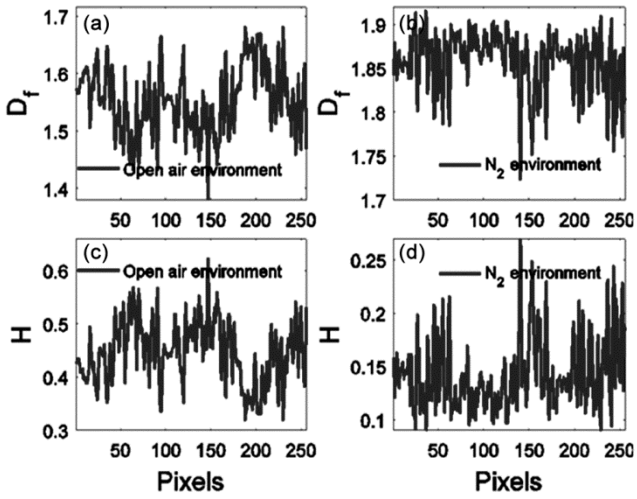

Fig. 4 — Fractal dimension (D_f) values for row pixels of perovskite surface (a) open air environment & (b) N_2 environment and Hurts exponent for (c) open air environment & (d) N_2 environment.

Figure 5(a) shows X-ray difractogram (XRD) of perovskite films fabricated in both open air environment and N_2 environment. The intensity of perovskite films corresponding to (110) and (220) plane in open air environment is stronger than that of N_2 environment. This shows that the crystallinity of perovskite films in open air environment is higher than that of N_2 environment. This may be due to the moisture assisted growth of perovskite crystal in open

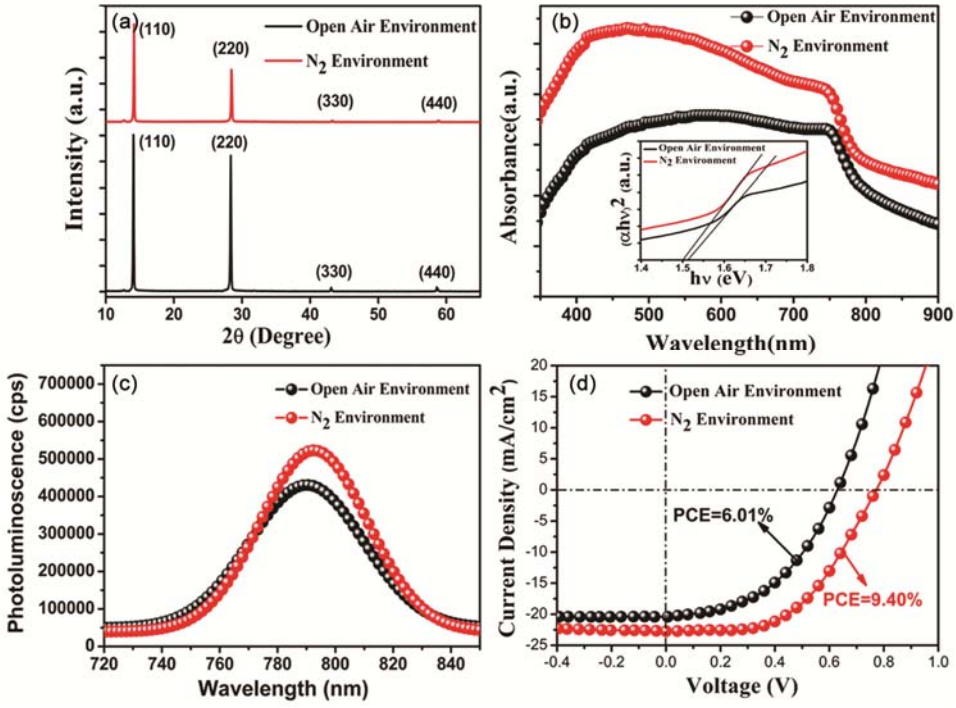

Fig. 5 — (a) X-ray difractogram, (b) absorbance spectra and inset is their Tauc's plots, (c) photoluminescence spectra and (d) J-V characteristic, of the perovskite thin films fabricated under different environmental conditions.

Table 1 — Photovoltaic parameters, fractal dimension and hurts exponent of our best device fabricated in both open air environment and N_2 environment.

Devices	J_{sc} (mA/cm^2)	V_{oc} (V)	Fill factor	Fractal dimension (D_f)	Hurst exponent (H)	PCE (%)
Open air environment	20.40	0.62	0.476	1.5561 ± 0.0549	0.4439 ± 0.0549	6.01
N_2 environment	22.50	0.76	0.547	1.8498 ± 0.0321	0.1502 ± 0.0321	9.40

air[39]. The XRD pattern of $CH_3NH_3PbI_{3-X}Cl_X$ indicates diffraction peaks at 14.1°, 28.4°, 43.2°, and 58.9° of 2θ degree positions, these peak positions are corresponding to the (110), (220), (330), and (440) lattice planes of the tetragonal crystal structure[40]. Figure 5(b) shows UV-Vis absorption spectra of $CH_3NH_3PbI_{3-X}Cl_X$ mixed halide perovskite films fabricated in open air environment as well as N_2 environment and inset shows their respective Tauc's plots. The absorbance of the perovskite films in N_2 environment increases as compare to open air environment. This improvement in the absorption spectra is due to the formation of compact, dense and voids free surface of perovskite thin films. The voids free uniform surface of perovskite thin films would stop the loss of light from the voids and enhance the absorption by internal light scattering and full trapping within the perovskite layer[41,42]. The optical band gap was calculated using Tauc's relation as

$$\alpha h\nu = A\,(h\nu - Eg)^{1/2} \quad \ldots (6)$$

The calculated value of band gap was found to be (1.50 eV) which is almost same in both the cases open air and N_2 environment as shown in inset of Fig. 5(b). Figure 5(c) shows the steady state photoluminescence (PL) spectra of perovskite thin films fabricated in both open air and N_2 environment. A significant improvement in PL intensity was observed for films grown in N_2 environment. This increment in PL intensity shows that quality of perovskite thin films was improved and defect density was reduced which play an important role for suppressing the non-radiative recombination within the light absorbing layer. Figure 5(d) shows the J-V characteristics of the devices fabricated in open air environment and N_2 environment. The photovoltaic parameters of our champion devices in both conditions are summarized in Table 1 along with fractal dimension and hurts exponent. The short circuit current density (J_{sc}), open circuit voltage (V_{oc}), fill factor (FF) and the PCE was found to be 22.50 mA cm^2, 0.76 V, 0.547 and 9.40%, respectively in N_2 environment while in the case of open-air environment it was 20 mA cm^2, 0.62 V, 0.476 and 6.01% respectively. The PCE in N_2 environment was much larger than that of open-air environment because of rougher surface formed in case of N_2 environment. This rougher surface offers a strong interfacing between $CH_3NH_3PbI_{3-X}Cl_X$ and P3HT layers which may be favourable for both internal light scattering as well as charge transportation[13].

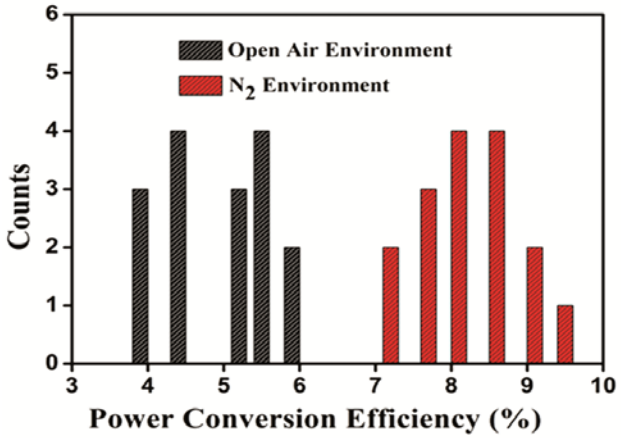

Fig. 6 — Histogram plot PCE of 16 devices fabricated in open air environment and 16 devices fabricated in N_2 environment.

Figure 6 shows the histogram plot of PCE of 16 devices fabricated in open air environment and N_2 environment. The average PCE was found to be 8.15% in N_2 environment and 5.01% in open air environment. These results confirm consistency as well as reproducibility of our devices under different environmental conditions.

Therefore, a drastic improvement of approximately 60% in PCE inside N_2 environment has been observed with enhanced J_{sc}, V_{oc} and FF in comparison to open air environment. Somewhat the PCE in open air environment was low because the charge carriers trapped within the voids. Thus, the fractal analysis techniques would be an effective way to investigate the deeper insight in to the surface morphology of perovskite thin films surface.

4 Conclusion

We have investigated a comparative study of $CH_3NH_3PbI_{3-X}Cl_X$ mixed halide perovskite solar cells fabricated in both open air environment as well as in

N_2 environment. The growth of $CH_3NH_3PbI_{3-X}Cl_X$ surface in both cases was found to be totally different. Fractal analysis was performed on SEM micrographs. It was observed that the estimated fractal dimension enhanced for $CH_3NH_3PbI_{3-X}Cl_X$ films grown in N_2 environment. Such surface is jagged which provides larger surface areas for photovoltaic device applications. These results suggest that the quality of $CH_3NH_3PbI_{3-X}Cl_X$ films as well as interfacing between $CH_3NH_3PbI_{3-X}Cl_X$ /P3HT layers has been improved in N_2 environment as compare to that in open air environment. Absorbance, PL intensity and photovoltaic performance of the devices were enhanced due to self-affine fractal structure. The power conversion efficiency in open air environment is 6.01% while in case of N_2 environment is found to be 9.40% which is approximately 60% improvement in PCE as compare to that of open air environment. The devices in both open air environment and N_2 environment are very consistence and reproducible. Thus, self-affine fractal structures of perovskite surface and its indentation are become a key factors for the determination of overall device performances of PSCs. Our results suggested that fractal analysis may be a useful technique for the investigations of perovskite solar cells in future.

Acknowledgements

MSP is thankful to University Grant Commission, New Delhi, India for providing financial support during the research work. The financial support to this work was provided by the Department of Science & Technology under DST-FIST and UGC-CAS Phase-II grants to Physics Department, University of Allahabad.

References

1 Kojima A, Teshima K, Shirai Y & Miyasaka T, *J Am Chem Soc*, 131 (2009) 6050.
2 Jung E H, Jeon N J, Park E Y, Moon C S, Shin T J, Yang T-Y, Noh J H & J Seo, *Nature,* 567 (2019) 511.
3 Chauhan A K & Kumar P, *J Mater Sci: Mater Electron,* 30 (2019) 9582.
4 Chaudhary D K, Kumar P & Kumar L, *Chem Phys Lett,* 685 (2017) 210.
5 Best-Research-Cell Efficiencies (National Renewable Energy Laboratory, (2020) *https://www.nrel.gov/pv/assets/pdfs/best-research-cell efficiencies. 20200406*. pdf
6 Chaudhary D K, Kumar P & Kumar L, *J Mater Sci: Mater Electron,* 28 (2017) 3451.
7 Liu Z, He T, Liu K, Wang J, Zhou Y, Yang J, Liu H, Jiang Y, Ma H & Yuan M, *J Mater Chem A,* 5 (2017) 24282.
8 Chiang C H & Wu C G, *Nat Photonics,* 10 (2016) 196.
9 Feng S, lv P, Ding D, Aa R, Liu T, Su P, Yang W, Yang J, Fu W & Yang H, *Vacuum,* 166 (2019) 255.
10 Patel M S, Chaudhary D K, Kumar P & Kumar L, *J Mater Sci: Mater Electron,* 31 (2020) 11150.
11 Chaudhary D K, Kumar P & Kumar L, *RSC Advances,* 6 (2016) 94731.
12 Jiang J, Wang Q, Jin Z, Zhang X, Lei J, Bin H, Zhang Z-G, Li Y & Liu S, *Adv Energy Mater,* 8 (2018) 1701757.
13 Cheng Y, Xu X, Xie Y, Li H-W, Qing J, Ma C, Lee C-S, So F & Tsang S-W, *Solar RRL,* 1 (2017) 1770131.
14 Akbulatov A F, Luchkin S Y, Frolova L A, Dremova N N, Gerasimov K L, Zhidkov I S, Anokhin D V, Kurmaev E Z, Stevenson K J & Troshin P A, *J Phys Chem Lett,* 8 (2017) 1211.
15 Yavari M, Mazloum-Ardakani M, Gholipour S, Tavakoli M M, Turren-Cruz S-H, Taghavinia N, Grätzel M, Hagfeldt A & Saliba M, *Adv Energy Mater,* 8 (2018) 1800177.
16 Deng K, Liu Z, Xin Y & Li L, *Adv Mater Interfaces,* 5 (2018) 1800499.
17 Liang J, Chen Z, Yang G, Wang H, Ye F, Tao C & Fang G, *ACS Appl Mater Interfaces,* 11 (2019) 23152.
18 Gao H, Bao C, Li F, Yu T, Yang J, Zhu W, Zhou X, Fu G & Zou Z, *ACS Appl Mater Interfaces,* 7 (2015) 9110.
19 Wang G, Liua D, Xiang J, Zhou D, Alameh K, Ding B & Song Q, *RSC Advances,* 6 (2016) 43299.
20 Raga S R, Jung M-C, Lee M V, Leyden M R, Kato Y & Qi Y, *Chem Mater,* 27 (2015) 1597.
21 Huang Y-C, Tsao C-S, Cho Y-J, Chen K-C, Chiang K-M, Hsiao S-Y, Chen C-W, Su C-J, Jeng U-S & Lin H-W, *Sci Rep,* 5 (2015) 13657.
22 Kavyashree, Pandey R K, Yadav R P, Kumar M, Bhasker H P, Mittal A K, Pandey A C & Pandey S N, *Appl Surf Sci,* 466 (2019) 780.
23 Yadav R P, Agarwal D C, Kumar M, Rajput P, Tomar D S, Pandey S N, Priya P K & Mittal A K, *Appl Surf Sci,* 416 (2017) 51.
24 Yadav R P, Kumar T, Mittal A K, Dwivedi S & Kanjilal D, *Appl Surf Sci,* 347 (2015) 706.
25 Ţălu Ş, Bramowicz M, Kulesza S, Dalouji V, Solaymani S & Valedbagi S, *Microsc Res Tech,* 79 (2016) 1208.
26 Ramamoorthy B, *Appl Surf Sci,* 280 (2013) 332.
27 Singh U B, Yadav R P, Kumar R, Ojha S, Mittal A K, Ghosh S & Singh F, *J Appl Phys,* 122 (2017) 185303.
28 Higuchi T, *Physica D,* 31 (1988) 277.
29 Cervantes-De la Torre F, Trejo J G, Real-Ramírez C & Hoyos-Reyes L, *J Phys: Conf Ser IOP Publ,* 475 (2013) 012.
30 Paramanathan P & Uthayakumar R, *Comput Biol Med,* 38 (2008) 372.
31 Sourina O, Wang Q, Liu Y & Nguyen M K, *Biosignals,* 1 (2011) 82.
32 Hinrikus H, Bachmann M, Karai D, Klonowski W, Lass J, Stepien P, Stepien R & Tuulik V, *Med Biol Eng Comput,* 49 (2011) 585.
33 Singh G, Yadav R P, Bhasker H P, Kumar M, Rajput P, Rao P N, Rai S K & Singh M K, *Mater Res Express,* 5 (2018) 126405.
34 Kavyashree, Yadav R P, Parveena S, Joshi L P & Pandey S N, *Mater Res Bull,* 120 (2019) 110574.
35 Liao H C, Tsao C S, Jao M-H, Shyue J J, Hsu C P, Huang Y C, Tian K Y, Chen C Y, Sue C J & Su W F, *J Mater Chem A,* 3 (2015) 10526.

36 Zheng L, Ma Y, Chu S, Wang S, Qu B, Xiao L, Chen Z, Gong Q, Wu Z & Hou X, *Nanoscale,* 6 (2014) 8171.
37 Yadav R P, Kumar M, Mittal A K & Pandey A C, *Chaos,* 25 (2015) 083115.
38 Pelliccione M & Lu T M, *Springer Series in Material Science, New York,* (2008).
39 Zhang K, Wang Z, Wang G, Wang J, Li Y, Qian W, Zheng S, Xiao S & Yang S, *Nat Commun,* 11 (2020) 1006.
40 Chauhan A K & Kumar P, *J Phys D: Appl Phys,* 50 (2017) 325105.
41 Oksengendler B L, Ashurov N R, Maksimov S E, Uralov I Z & Karpova O V, *Nanosyst Phys Chem Math,* 8 (2017) 92.
42 Wang Y C, Li H, Hong Y H, Hong K B, Chen F C, Hsu C H, Lee R K, Conti C, Kao T S & Lu T C, *ACS Nano,* 13 (2019) 5421.